

RSC Advances



This is an *Accepted Manuscript*, which has been through the Royal Society of Chemistry peer review process and has been accepted for publication.

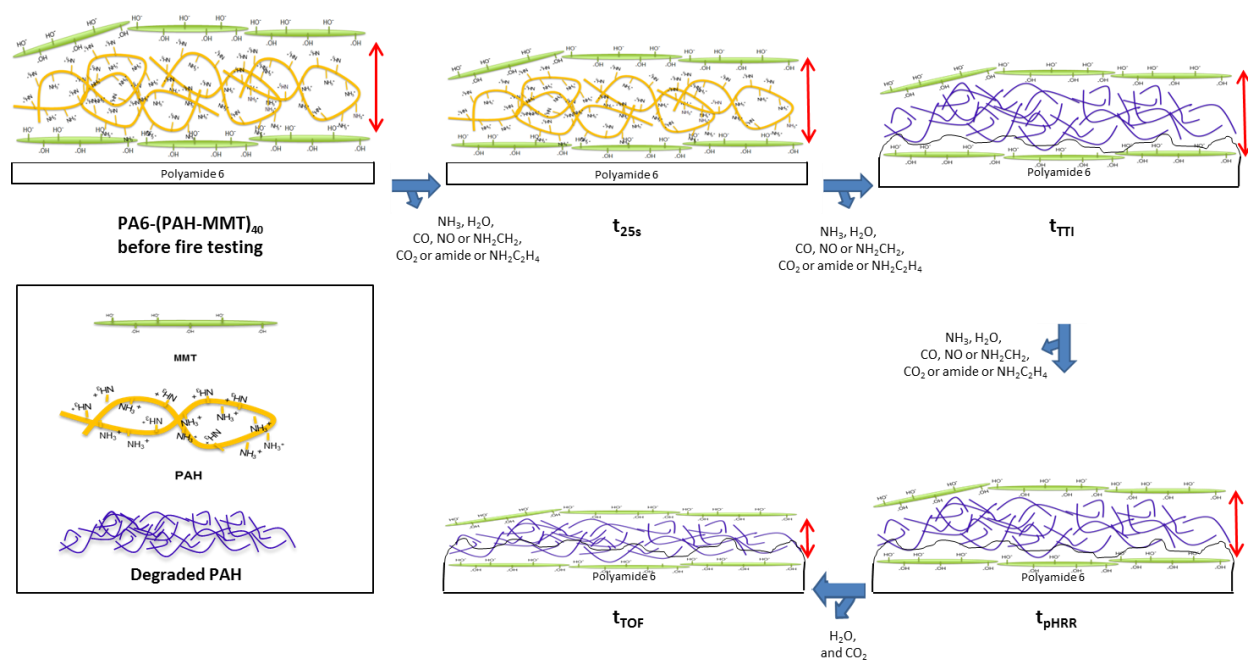
Accepted Manuscripts are published online shortly after acceptance, before technical editing, formatting and proof reading. Using this free service, authors can make their results available to the community, in citable form, before we publish the edited article. This *Accepted Manuscript* will be replaced by the edited, formatted and paginated article as soon as this is available.

You can find more information about *Accepted Manuscripts* in the [Information for Authors](#).

Please note that technical editing may introduce minor changes to the text and/or graphics, which may alter content. The journal's standard [Terms & Conditions](#) and the [Ethical guidelines](#) still apply. In no event shall the Royal Society of Chemistry be held responsible for any errors or omissions in this *Accepted Manuscript* or any consequences arising from the use of any information it contains.

Text and graphical abstract

The efficiency of a flame retardant coating based on poly(allylamine) (PAH) and montmorillonite (MMT), deposited on polyamide 6 (PA6) bulk polymer, was demonstrated in our previous work. In this paper we aim at investigating the action's mechanism of this flame retardant coating. To reach this objective, PA6-(PAH-MMT) at 40 bilayers was tested in cone calorimeter and interrupted at different characteristic times: 25s (after the fire test starting), time to ignition, peak heat release rate and time of flameout. The condensed phase of specimen residues obtained were characterized by scanning electron microscopy, X-ray diffraction, laser desorption ionization and solid state ^{13}C nuclear magnetic resonance while the gas phase was evaluated by thermogravimetric analysis coupled with infrared spectroscopy and mass spectrometer. Finally the pyrolysis combustion flow calorimeter was used to evidence the effect of this Layer-by-Layer assembly in gas phase. A possible mechanism explaining the improvement of the flame retardancy of a PA6 substrate in the presence of LbL coating made of PAH and clay is proposed.



ARTICLE

Mechanistic investigation of flame retardant coating made by Layer-by-Layer

Cite this: DOI: 10.1039/x0xx00000x

K. Apaydin,^{a, b*} A. Laachachi,^{a*} T. Fouquet,^a M. Jimenez,^b S. Bourbigot^b and D. Ruch^a,

Received xxth January 2014,
Accepted xxth January 2014

DOI: 10.1039/x0xx00000x

www.rsc.org/advances

The efficiency of a flame retardant coating based on poly(allylamine) (PAH) and montmorillonite (MMT), deposited on polyamide 6 (PA6) bulk polymer, was demonstrated in our previous work. In this paper we aim at investigating the action's mechanism of this flame retardant coating. To reach this objective, PA6-(PAH-MMT) at 40 bilayers was tested in cone calorimeter and interrupted at different characteristic times: 25s (after the fire test starting), time to ignition, peak heat release rate and time of flameout. The condensed phase of specimen residues obtained were characterized by scanning electron microscopy, X-ray diffraction, laser desorption ionization and solid state ¹³C nuclear magnetic resonance while the gas phase was evaluated by thermogravimetric analysis coupled with infrared spectroscopy and mass spectrometer. Finally the pyrolysis combustion flow calorimeter was used to evidence the effect of this Layer-by-Layer assembly in gas phase. A possible mechanism explaining the improvement of the flame retardancy of a PA6 substrate in the presence of LbL coating made of PAH and clay is proposed.

1. Introduction

In recent years, Layer-by-Layer (LbL) assembly has become a popular deposition technique to design flame retardant coatings on different kind of substrates such as textiles¹⁻⁴, polyurethane foams^{5, 6}. Montmorillonite (MMT) was widely used as polyanion in the LbL flame retardant coatings. In fact, this phyllosilicate has been coupled with various polycations such as branched polyethylenimine, poly(N-benzyloxycarbonyl-3,4-dihydroxyphenylalanine), chitosan, poly(allylamine), to improve the flammability of cotton⁷, polyimide fabrics³, polyurethane foam⁸ and polylactic acid film⁹, respectively. Our group has firstly showed the efficiency of clay based flame retardant coatings deposited onto thermoplastics⁹. In a previous paper¹⁰, we showed the efficiency of a flame retardant coating based on poly(allylamine) (PAH) (as polycation) and montmorillonite (MMT) (as polyanion) deposited at the surface of polyamide 6 film. Indeed, cone calorimetry evidenced excellent reaction to fire of the material since the peak of heat release rate (pHRR) was decreased by more than 60% in the presence of (PAH-MMT) film in comparison with pristine polyamide 6. Moreover a continuous charred layer was observed during the combustion and the thickness of the coating at the end of

the fire test was twice higher than the initial thickness. The expanded charred layer at the surface of polyamide 6 was assumed acting as protective layer limiting heat and mass transfer¹⁰. Nevertheless the mechanism of Layer-by-Layer flame retardant coatings has never been fully investigated into details and it is one of the goals of this paper. Thus, a (PAH-MMT) coating was elaborated using Layer-by-Layer assembly and tested by cone calorimetry. During the experiment, the cone calorimeter was interrupted at different characteristic times: at 25s after starting, at time to ignition, at time of peak of heat release rate and at time of flameout. The specimen residues were then removed from cone calorimeter and both condensed and gas phases were analyzed with scanning electron microscopy (SEM), X-ray diffraction (XRD), laser desorption ionization (LDI) mass spectrometry, ¹³C nuclear magnetic resonance (NMR), thermogravimetric analysis coupled with infrared spectroscopy and mass spectrometer (TGA-FTIR and TGA-MS) and pyrolysis combustion flow calorimeter (PCFC). Mechanism explaining the improvement of the flame retardancy of a PA6 substrate in the presence of LbL coating made of PAH and clay is investigated in this paper.

2. Experimental

2.1. Materials

Poly(allylamine) hydrochloride (PAH) (Sigma Aldrich, $M_w = 120\,000 - 200\,000\text{ g.mol}^{-1}$) was dissolved at 1 mg.mL^{-1} in 50 mM tris(hydroxymethyl) aminomethane (Euromedex, $M_w = 121,1\text{ g.mol}^{-1}$) buffer (pH adjusted to 7.5 with hydrochloric acid, Acros Chemicals, 36.5-37%). Sodium montmorillonite (Na^+ -MMT) (from Southern Clay Co) was dispersed at 1 % (w/v) in water whose pH was adjusted to $10 (\pm 0.1)$ with a diluted sodium hydroxide solution (Acros Chemicals). This suspension was then sonicated for 1h in an ultrasonic bath to ensure proper exfoliation of the clay. No sedimentation was observed even after several days of storage in the absence of stirring. All solutions were prepared from doubly distilled water (Millipore Simplicity system, $\rho = 18.2\text{ M}\Omega.\text{cm}$). Polyamide 6 (PA6) sheets with a thickness of $500\text{ }\mu\text{m}$ and a density of 1.14 g.cm^{-3} were purchased from Goodfellow (Cambridge, England) and were used as received for thermal degradation and fire resistance characterizations.

2.2. Layer by Layer elaboration

The polyamide 6 substrate was immersed alternatively into solutions containing positive (PAH) and negative (MMT) species corresponding to one (PAH-MMT) bilayers (BL). Between each immersion step, the substrate was rinsed with the buffer solution and water solution. The buffer and water rinse steps aimed desorbing weakly adsorbed PAH and clay, respectively. The adsorption and rinsing step times were set at 1 min. The samples were not blown dry between successive deposition steps. After 40 BL elaborated, the sample was rinsed in water and put in the oven at $60\text{ }^\circ\text{C}$ for 24 hours.

2.3. Reaction to fire

a. Cone calorimeter

The fire properties were studied using a cone calorimeter device (Fire Testing Technology) following the procedure defined in ISO 5660-1. Various parameters were measured by the cone calorimeter: time to ignition (TTI), time of flameout (TOF), heat release rate (HRR) as a function of time, peak of heat release rate (pHRR), total heat release (THR), time to pHRR (t_{pHRR}), mass loss rate (MLR) and total smoke released (TSR). HRR, TTI, THR and TSR of uncoated and coated polyamide 6 were examined. A $50 \times 50 \times 0.5\text{ mm}^3$ sample was exposed under an external heat flux of 25 kW/m^2 . The specimen was placed in an aluminium foil pan that was laid on cone calorimeter sample holder. This low heat flux was chosen as we work with thin materials. With higher heat flux, the effect of coatings cannot be clearly observed. All experiments were repeated in triplicate to check the repeatability. To investigate the action's mechanism of our coatings, the cone calorimeter test was stopped at

different times: t_{25s} , t_{TTI} , t_{pHRR} and t_{TOF} (Fig 1) and the resulting residues were taken out of the cone to be characterized. The samples self-extinguished after being removed from cone calorimeter.

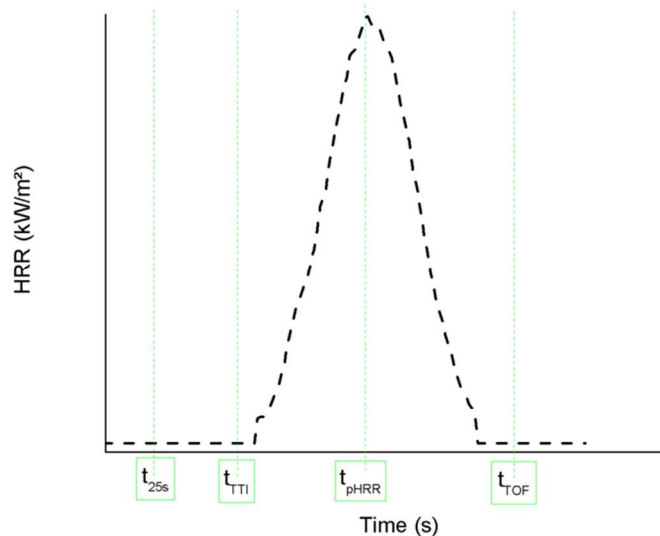


Fig 1 Schematic representation of the different times where the cone calorimeter test was interrupted: t_{25s} , t_{TTI} , t_{pHRR} and t_{TOF} .

b. Pyrolysis-combustion flow calorimetry (PCFC)

The Heat Release Rate (HRR) in W/g and the decomposition temperature ($^\circ\text{C}$) was studied using a Pyrolysis Combustion Flow Calorimeter (PCFC) device (Fire Testing Technology, UK), according to ASTM D7309 method A. The mass of each sample was between 4 and 8 mg and the test was performed under nitrogen atmosphere with a heating rate of $1\text{ }^\circ\text{C/s}$ from 20 to $600\text{ }^\circ\text{C}$. The samples were carefully cut with scissors and only well-covered area of samples was tested in PCFC because the coatings come off after cutting on some area of sample. All the experiments were repeated in triplicate and the values are reproducible within $\pm 2\%$.

2.4. Analysis of the condensed phase

The structure of residues were determined by X-ray diffraction (XRD) using a Panalytical X'Pert Pro MPD diffractometer (Almelo, Netherlands) in grazing incidence configuration using the $\text{Cu K}\alpha$ radiation ($\lambda = 1.5405\text{ \AA}$, starting angle is 3 ° , step size $0,050^\circ$ at 3 min^{-1}). The beam was generated at 40 kV and 45 mA. A parabolic mirror and Pixel detector were used as incident and secondary optics, respectively. The samples were put directly onto the sample holder of XRD instrument and the charred surface of the samples was analyzed. The morphology was imaged by Scanning Electron Microscopy (SEM) with an environmental microscope (FEI-Quanta 200 type) at an accelerating voltage of 10 kV, magnification $\times 150$, $\times 200$ and $\times 2000$. The final residues were also analyzed by ^{13}C solid state NMR. The NMR spectrometer was a Bruker Avance II equipped with a 4

mm probe and working at 100.6 MHz with cross polarization ^1H - ^{13}C and dipolar decoupling with magic angle spinning (MAS with a frequency of 12 kHz). In addition, Laser Desorption Ionization (LDI) mass spectra were recorded using a Bruker Autoflex III mass spectrometer (Bruker Daltonics, Bremen, Germany) equipped with a frequency-tripled Nd-YAG laser ($\lambda=355\text{ nm}$) operating at a pulse rate of 50 Hz. Residues were mass-analyzed using a positive 19 kV voltage with a 10 ns Pulsed Ion Extraction. The Time-of-Flight analyzer was operated in reflection mode and ions were detected using a microchannel plate detector. External calibration was performed with a poly(ethylene glycol) PEG 600 g/mol standard (Sigma Aldrich, St Louis, MO) analyzed in a solvent-free sample preparation, with a hydroxycinnamic acid (CHCA, Bruker Daltonics) as matrix and Lithium trifluoroacetate (LiTFA, Sigma Aldrich) as cationization salt. FlexControl software version 3.0 (Bruker Daltonics) was used for instrument control and data acquisition, while both FlexAnalysis software version 3.0 (Bruker Daltonics) and mMass version 5.5¹¹ were used for data processing.

2.5. Analysis of the decomposition gases

The Fourier transform infrared (FTIR) spectroscopy has been employed to analyze evolved gases during thermogravimetric analysis. The FTIR device is a Bruker Optics Tensor 27 spectrometer working in the range: $4000 - 600\text{ cm}^{-1}$ (32 scans and 4 cm^{-1} resolution) (Fig. 2). The thermal stability of the coatings and their effect on substrate were investigated by thermogravimetric analysis (TGA). TGA apparatus was a NETZSCH-STA 409 PC, operating in argon under a $100\text{ cm}^3\cdot\text{min}^{-1}$ gas flow using open alumina crucibles containing approximately 10 mg of sample. The run was carried out in dynamic conditions at a constant heating rate of $10\text{ }^\circ\text{C}\cdot\text{min}^{-1}$ between 30 and $1000\text{ }^\circ\text{C}$ (Fig. 2). The MS 403C Aeolos mass spectrometer (MS) from NETZSCH was also used to analyze the gas components which are emitted during the thermogravimetric experiments. The transfer lines between TGA/FTIR and TGA/MS were heated at $230\text{ }^\circ\text{C}$ and $250\text{ }^\circ\text{C}$ respectively to avoid the condensation reaction at the interfaces. All products were identified using NIST library. The different ion currents followed by the MS device are summarized in the Table 1.

Ion current selected	m/z of main peak	m/z of second peak
$\text{NH}_3^{+\bullet}$	17	15 ($\text{NH}^{+\bullet}$)
$\text{CO}^{+\bullet}$	28	-
$\text{CO}_2^{+\bullet}$ or $\text{CONH}_2^{+\bullet}$ or $\text{NH}_2\text{C}_2\text{H}_4^{+\bullet}$	44	-
$\text{H}_2\text{O}^{+\bullet}$	18	17
$\text{NO}^{+\bullet}$ or $\text{NH}_2\text{CH}_2^{+\bullet}$	30	46 for $\text{NO}^{+\bullet}$
$\text{CH}_4^{+\bullet}$	16	15

Table 1 Mass/charge (m/z) of selected ion current.

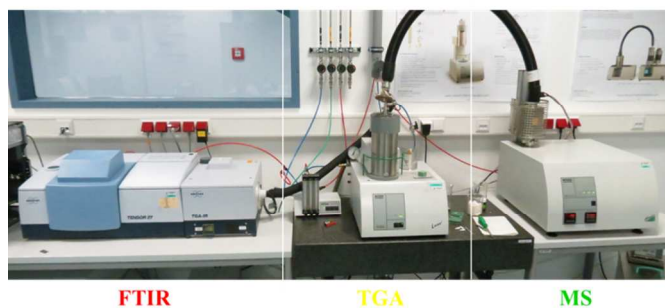


Fig 2 Coupling of FTIR-TGA-MS instruments.

3. Results

3.1. Reaction to fire: cone calorimeter results

The reaction to fire of polyamide 6 uncoated and coated with (PAH-MMT) at 40 bilayers was assessed by cone calorimeter under external flux of 25 kW/m^2 . Fig. 3 shows the heat release rate (HRR) as function of time for untreated and treated polyamide 6 with (PAH-MMT)₄₀ assemblies.

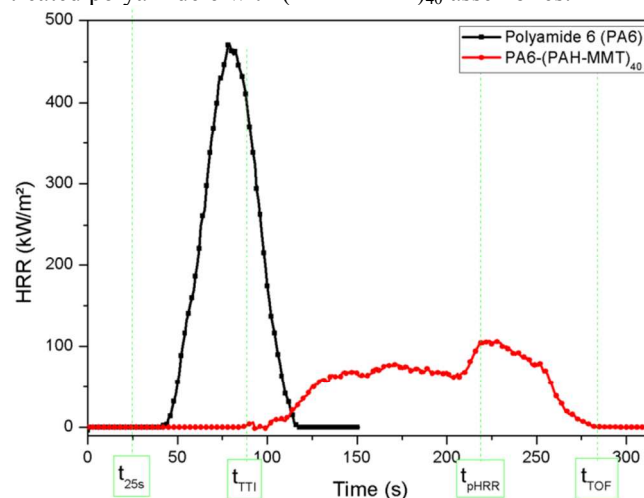


Fig 3 Cone calorimeter results of pristine PA6 and PA6 coated with 40 bilayers assemblies.

The fire properties of polyamide 6 coated at different number of bilayers (5, 10 and 20 BL) have already been discussed in our previous work¹⁰ wherein PA6 coated with (PAH-MMT)₂₀ assemblies displayed a maximum peak Heat Release Rate (pHRR) of $197 \pm 96\text{ kW/m}^2$. Herein, a (PAH-MMT) at 40 bilayers exhibits better results, *i.e.* a maximum pHRR of $133 \pm 3\text{ kW/m}^2$. Using these 40 BL samples, cone calorimeter test was then stopped at critical times: 25s after test starting, time to ignition (TTI), pHRR and time of flameout (TOF). The different sample residues obtained were taken out of the cone to be characterized. Fig. 4 exhibits the pictures of sample residues before fire testing and at 25s, TTI, pHRR and TOF.

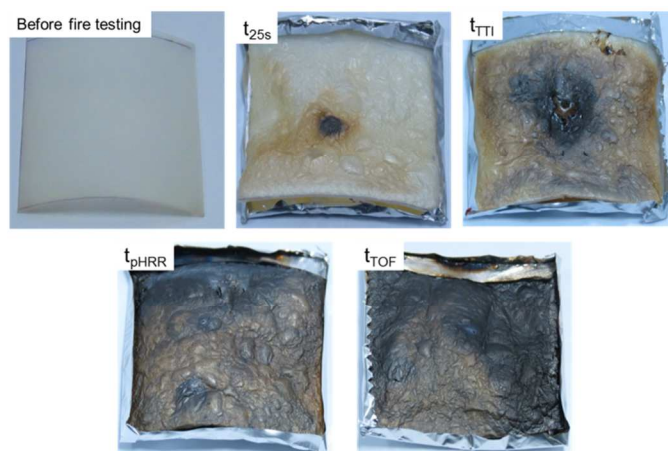


Fig 4 Images of coated PA6 before fire testing and resulting residues stopped: t_{25s} , t_{TTI} , t_{pHRR} and t_{TOF} .

The observation of sample before fire testing and resulting residues is particularly interesting. It can be clearly evidenced that the appearance of sample modify as a function of exposure time. Before fire testing, polyamide 6 coated with (PAH-MMT) assembly exhibits a smooth and regular surface (initially “beige” due to the MMT). At 25s the sample appearance changes: the surface color becomes yellowish and we observe the presence of small bubbles randomly distributed on the surface. At TTI, the specimen color is more tanned and the size of small bubbles, previously observed at 25s, increases to form larger bubbles. At pHRR and TOF, the larger bubbles formed will contribute to the formation of intact “brown-black” carbonaceous char layer at the surface of polyamide 6, already observed for (PAH-MMT)₂₀ coatings¹⁰.

3.2. Condensed phase analysis

The sample residues at 25s, TTI, pHRR, TOF and prior to burning were imaged by SEM (Fig. 5). All samples show an ordered sheets structure at different interrupted time. The coating begins to swell at time to ignition and interacts physically with the substrate from the maximum of heat release rate. EDX mapping was performed in order to examine the potential interaction between the MMT based coating and polyamide substrate (Fig. 6). In fact the substrate is constituted of carbon, oxygen and nitrogen while the MMT is composed of aluminum, silicon, oxygen...elements. The presence of these elements, in the entire samples, evidences the elemental diffusion of coating with the melted substrate (Fig. 6).

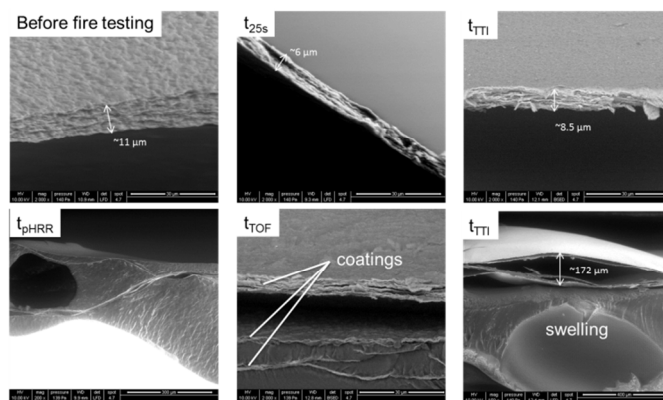


Fig 5 SEM images of coated PA6 before fire testing (A) and sample residues at 25s (B), TTI (C) and (F), pHRR (D) and TOF (E).

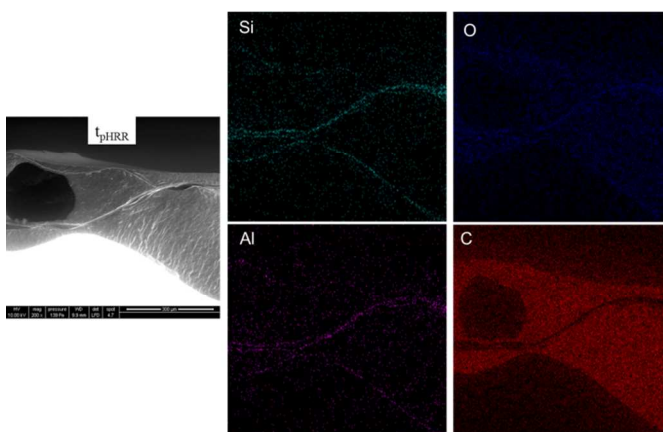


Fig 6 SEM images and elemental analysis (Si, O, Al and C) of (PAH-MMT)₄₀ samples at pHRR.

The structure analysis of neat MMT powder, (PAH-MMT)₄₀ coating and samples residues at different times was performed by XRD (Fig. 7). The peak at 7.2° for neat MMT powder derives from a basal spacing of 12.1 \AA which is the distance between two platelets. The diffraction peak of (PAH-MMT)₄₀ coating prior to burning appears to be 6.0° with an interplanar spacing of 14.4 \AA . As observed in our previous paper¹², this increase of basal spacing between platelets is due to the intercalation of the PAH between the clay sheets⁷. At 25s the diffraction peak is similar ($2\theta = 6.0^\circ$ and $d_{hkl} = 14.6\text{ \AA}$) to coating prior to burning which confirms the presence of PAH between the sheets. From TTI to TOF, the diffraction peaks is shifted to higher 2θ and the basal spacing decreases up to 13.4 \AA (for sample residue at TOF). This decrease of distance between platelets can be explained by the degradation of PAH buried in the platelets during the fire testing. Moreover, the collapse of clay d-spacing when the material is heated fits with the mechanistic findings of clay nanocomposites in bulk form.¹³ The degradation of poly(allylamine) during combustion reaction as it occurs from TTI will be examined

on the one hand by LDI and on the other hand by TGA coupled with FTIR and MS experiments.

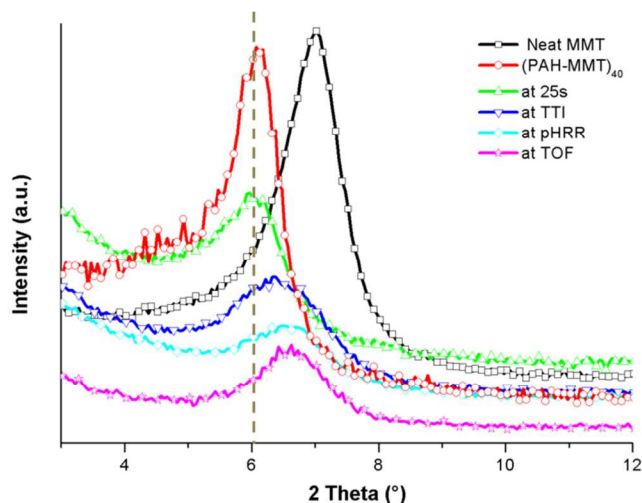


Fig 7 X-Ray diffraction patterns of neat MMT and (PAH-MMT)₄₀ films at 25s, TTI, pHRR and TOF

Positive LDI mass spectra of MMT, PAH, PA6-(PAH-MMT)₄₀ prior to burning and residues at 25s, TTI, pHRR and TOF are depicted in Fig. 8. Three unidentified peaks are readily detected from the native MMT sample at m/z 270, m/z 393 and m/z 449, highly suspected to be at the surface of the clay product, or as an intercalated pollutant. It constitutes at least the fingerprint of a pristine MMT surface. The MALDI mass spectrum of MMT (using CHCA as matrix to promote the detection of intercalated species¹⁴) did not allow those unidentified products to be better observed but gave rise to sodiated CHCA adducts only (Fig. S1 and Table S1, Supporting Information) highlighting the sodium intercalation expected for a MMT.

The LDI mass spectrum of poly(allylamine) (PAH) recorded in the positive mode exhibits its own typical pattern recorded in the low mass range, with several peaks spaced by 12 Da readily detected (Table S2a, Supporting Information). Post Source Decay (PSD) LDI-MS spectra showed clear filiations between peaks from this fingerprint, the largest species yielding the smallest peaks under high laser fluence activation (Fig. S2, Supporting Information). LDI-MS pattern of PAH is thus formed of fragments from in-chain scissions and several In Source Decay (ISD) fragments. These peaks are not found in the coated PA6 sample prior to burning test, probably deeply intercalated within the clay platelets, while the MMT pattern is readily seen (Fig 8, PA6-(PAH-MMT)₄₀). On the opposite, both MMT and PAH patterns are found in the residue at 25s, as if the first seconds of burning would allow the intercalated PAH to reach the surface or the clay platelets to slightly expand hence facilitating the PAH chains detection. Degradation of PAH chains is pointed out at TTI by the observation of additional peak series spaced by ± 12 Da in the low mass range (Table S2b, Supporting

Information), while neither the original LDI pattern of PAH nor the MMT pattern are found. The LDI mass spectrum of the residue at pHRR still exhibits the peak series observed in the previous sample and suspected to arise from degraded PAH, concomitantly with a dense peak distribution covering the whole mass range, typical of a carbonaceous char layer. Finally at TOF, the relative abundance of the peaks related to a degraded PAH dramatically decreases while the char pattern (dense peak distribution) now becomes the major signal.

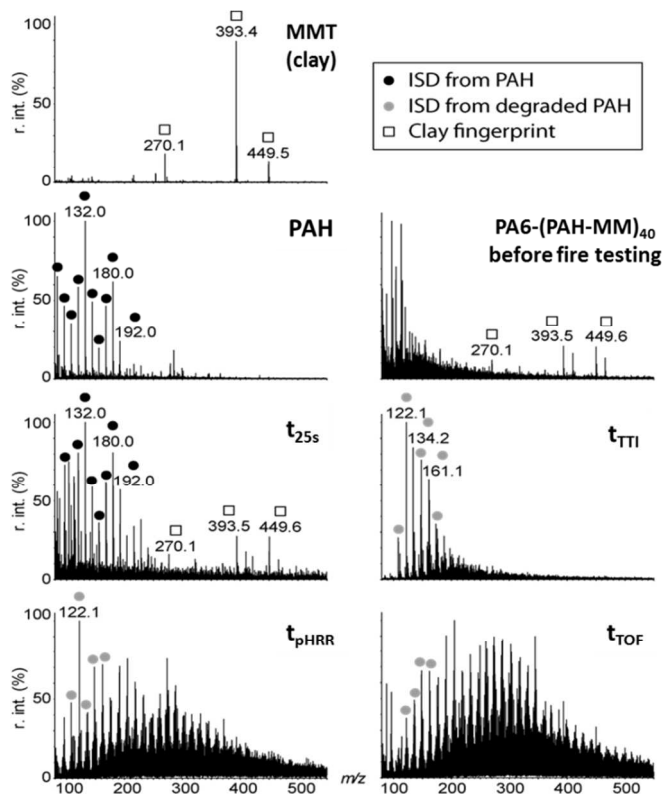


Fig 8 LDI mass spectra of MMT, PAH, PA6-(PAH-MMT)₄₀ prior to any burning tests and specimen residues at 25s, TTI, pHRR and TOF, recorded in the positive mode.

Fig 9 presents ¹³C CPMAS NMR spectra of the pristine polyamide 6, PA6-(PAH-MMT)₄₀ before fire testing and residues obtained at 25s, TTI, pHRR and TOF. The different carbons (C1, C2, C3, C4, C5 and C6) of the PA6 are labeled on the spectra and the peaks are attributed according to literature^{15, 16}. Pure polyamide 6 exhibits a chemical shift at 173.3 ppm attributed to carbon of C=O groups and four peaks (C2, C3, C4-C5 and C6) between 25 and 45 ppm corresponding to aliphatic carbons¹⁶. Otherwise, the peaks of coated polyamide are slightly shifted in comparison to uncoated polyamide 6 (Table 2). From resulting residue at 25s to TOF we distinguished a peak at 39.4 ppm (see zoom in Fig. 9). Therefore, the spectral fingerprint of polyamide 6 was found at the end of combustion (corresponding to the sample residue at TOF). According to the appearance of spectra and chemical shifts obtained, the polyamide 6 substrate moves from a γ phase to a thermodynamically more stable α phase crystalline structure¹⁷.

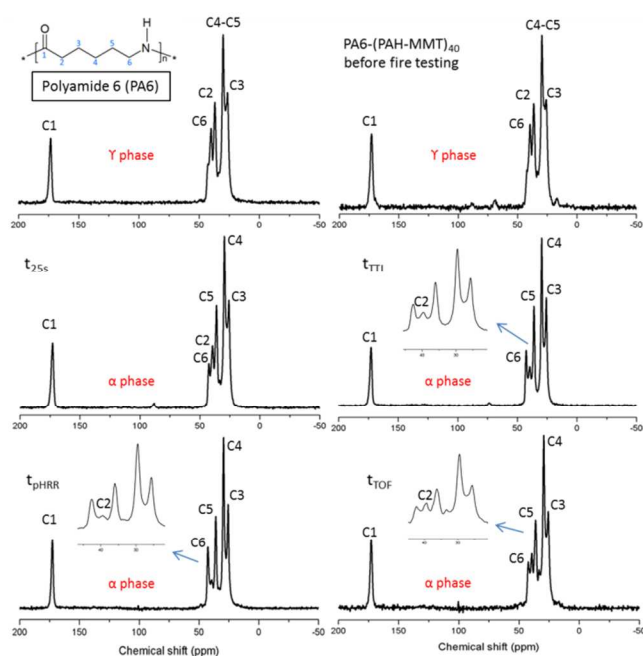


Fig 9 ^{13}C NMR spectra of the PA6, PA6-(PAH-MMT) $_{40}$ before fire testing and sample residues at 25s, TTI, pHRR and TOF.

Phase	Samples	C1	C2	C3	C4	C5	C6
Y	Polyamide 6 (PA6)	173.3	36.9	26.4	30.2	30.2	40.2
Y	PA6-(PAH-MMT) $_{40}$ before fire testing	173.0	36.5	25.9	36.4	36.4	39.6
α	t_{25s}	173.0	39.4	25.8	30.0	36.0	42.4
α	t_{TTI}	172.6	39.4	25.6	29.6	35.9	42.6
α	t_{pHRR}	172.9	39.4	25.6	29.5	36.1	42.8
α	t_{TOF}	172.9	39.4	25.8	29.5	36.3	42.3

Table 2 Assignments of the bands

The thermal stability of pristine polyamide 6, (PAH-MMT) $_{40}$ coatings, PA6-(PAH-MMT) $_{40}$ sample, poly(allylamine) powder and specimen residues at 25s, TTI, pHRR and TOF was evaluated by thermogravimetry analysis (TGA) (Fig. 10 and 11). Fig. 10 shows the residual weight as a function of temperature of different samples tested. According to literature¹⁸, in the absence of nucleophile such as water, the thermal decomposition of polyamide 6 at temperature higher than 300°C evolves mainly ϵ -caprolactame (monomer), polymer chain end-groups, cyclic oligomers and small gaseous molecules. Under argon atmosphere, the neat polyamide 6 film undergoes three thermal degradation steps. The first step around 100 °C is obviously due to desorption of water. The second peak, also observed in our previous work¹⁰, occurs between 350 and 500 °C corresponds to the main decomposition step of polyamide. The last step from 500 to 600 °C corresponds to the degradation of products formed during the second step. The thermal degradation of (PAH-

MMT) $_{40}$ coatings also proceeds by three steps. The first weight loss at 100°C is related to the adsorbed water. The second weight loss is located between 200 and 300 °C (temperatures at which PAH starts to degrade). It can be related to a small amount of PAH that was unaffected by the clay and decomposed spontaneously¹⁹. The last weight loss taking place from 550 to 700 °C is attributed to the dehydroxylation of structural AlOH groups of MMT²⁰. The coated polyamide 6 exhibits the same weight loss behaviour of pristine polyamide with a slight increase of residue amount (~2 % at 900°C). Furthermore all specimen residues at 25s, TTI, pHRR and TOF exhibits two degradation steps: the first step, which occurs at 440 °C (maximum degradation rate determined from DTG curves) is attributed to the degradation of polyamide 6 which was protected by the coatings during the combustion in cone calorimeter test and the second step is located between 500 and 600 °C corresponding to the degradation of the residue resulting from the first step. At 900 °C, no residue was observed for the pristine polyamide 6 and PAH contrary to the specimen residues at 25s, TTI, pHRR and TOF which left 4, 5, 7 and 71 % (we find the same residual mass of (PAH-MMT) $_{40}$ at the end of TG analysis) of residue, respectively. This increase of amount of residue at the end of TGA analysis evidences an evolution of organic-inorganic balance of the sample as function of the combustion time: the amount of inorganic compounds (such as MMT) increases compared to organic compounds (such as PAH, PA6) during the cone calorimeter test. Finally, the neat (PAH-MMT) $_{40}$ coating exhibits an residual amount of 72 % corresponding to all the inorganic compounds, and in particular MMT which display 85 % of residue. The difference of amount of residue between neat coatings and MMT can be explained by the presence of PAH inside the platelets which did not degrade earlier.

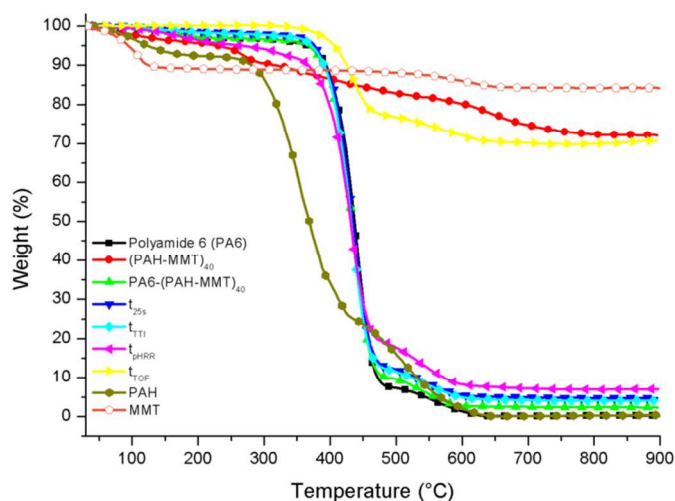


Fig 10 TGA curves under argon (heating rate: 10°C min $^{-1}$) of pristine polyamide 6, (PAH-MMT) $_{40}$, PA6-(PAH-MMT) $_{40}$, PAH, MMT and specimen residues at t_{25s} , t_{TTI} , t_{pHRR} , t_{TOF} .

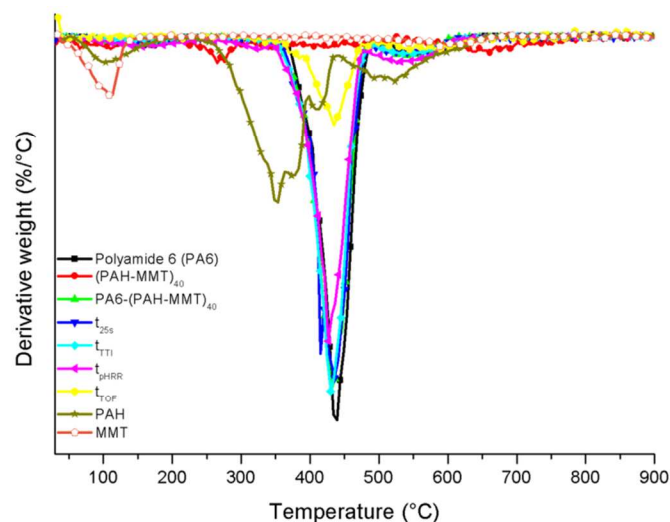


Fig 11 DTG curves of pristine polyamide 6, (PAH-MMT)₄₀, PA6-(PAH-MMT)₄₀, PAH, MMT and specimen residues t_{25s} , t_{TTI} , t_{pHRR} , t_{COF} .

After a study of the condensed phase, it was also important to concentrate on the study of the gas phase in order to obtain more information about the mechanism of the Layer-by-Layer flame retardant coatings.

3.3. Gas phase analysis

The TGA was coupled with infrared spectroscopy and mass spectrometry in order to study the evolved gases released during the thermal degradation. Fig. 12 shows the FTIR spectra of evolved gases during the thermal decomposition of pristine polyamide, PA6-(PAH-MMT)₄₀ prior to burning and specimen residues at 25s, TTI, pHRR and TOF. All the bands are labeled on the spectra and assigned according to the literature^{21,22} (Table 3).

Wavenumber (cm ⁻¹)	Assignment	References
670 and 2357	CO ₂	
712	Amide V (NH out of plane)	[21]
931, 961 and 3336	NH ₃	
1510	Amide II (NH deformation)	[20, 22]
1627 and 1713	Amide I (C=O stretching)	[20-22]
2958	CH ₂ asym. stretch	[21]
3333	N-H stretch	[21]
3500-3750	H ₂ O	

Table 3 Assignment of vibrations obtained by FTIR-TGA-MS experiment for PA6, PA6-(PAH-MMT)₄₀ and specimen residues at 25s, TTI, pHRR and TOF.

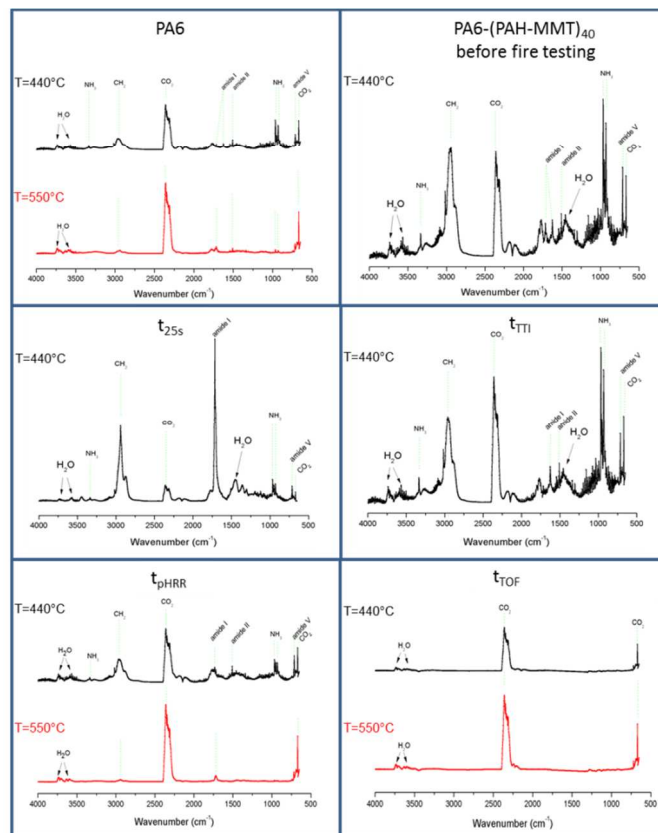


Fig 12 FTIR spectra of gases released during thermal degradation of PA6, PA6-(PAH-MMT)₄₀ and specimen residues at 25s, TTI, pHRR and TOF.

From TGA analysis, two characteristic temperatures could be evidenced: 440°C and 550°C (maximum degradation rate determined from DTG curves) corresponding to the main degradation steps taking place between 350°C and 500°C and the last decomposition step occurring between 500°C and 600°C, respectively. It is noted that no FTIR signal was detected at 550°C for PA6-(PAH-MMT)₄₀ prior to burning and specimen residues at 25s and TTI, probably due to the low amount of gaseous molecule released. The presence of water was detected in the 3500 - 3750 cm⁻¹ range as well as around 1430 cm⁻¹. At 440°C, the polyamide 6 releases mainly water, CO₂ (670 and 2357 cm⁻¹), NH₃ (931, 961 and 3336 cm⁻¹), hydrocarbons (2958 cm⁻¹) and amide groups (1627, 1713, 1510 and 712 cm⁻¹) while at 550°C the intensity of all previously detected peaks is significantly reduced except for the CO₂ bands. The presence of (PAH-MMT)₄₀ coating increases the intensity of all peaks detected for pristine polyamide 6 at 440°C. In particular, the increase of ν_{NH_3} , ν_{CH_2} and amide I-II bands is probably due to the presence of PAH whose characteristic peaks have already been identified by Laachachi et al.⁹ For the specimen residue at 25s an opposite trend compared to coated PA6 sample is observed, indeed, except for the amide I band the intensity of all detected signals decrease. At TTI hydrocarbon group, NH₃, CO₂, and amide I, II, V groups are produced intensely then at pHRR the amount of these products decreases significantly and at TOF

only CO₂ products are detected. From these findings, it is evidenced that from TTI different gaseous molecules such as NH₃, CH₂, amide groups are released providing from poly(allylamine) and polyamide and that the intensity of these same gases will decrease substantially up to disappear at TOF. These results are in agreement with XRD and LDI experiments. As FTIR spectra give main information about the chemical group present in the evolved gases released during the degradation we used mass spectrometry was used in order to support these statements.

Fig. 13 shows the different ion current signals of PA6, (PAH-MMT)₄₀, PA6-(PAH-MMT)₄₀ and specimen residues at 25s, TTI, pHRR and TOF as a function of temperature. Referring to the different gases species detected by FTIR and literature^{23, 24}, it was decided to follow some ions which could be released during the decomposition reaction. As it happens selected ions are: methane (*m/z* 16), ammonia (*m/z* 17), water molecule (*m/z* 18), carbon monoxide (*m/z* 28), nitric oxide or NH₂CH₂ chains (*m/z* 30) and dioxide carbon or NH₂C₂H₄ chains (*m/z* 44). Identification of species is based on the spectrum recorded from NIST database. For example two peaks (*m/z*=17 and *m/z*=18) are detected for water molecule in NIST database; therefore, to affirm the presence of water molecule these two signals at 17 and 18 *m/z* should be observed. We applied this rule to identify the different species. Looking at MS spectra, three temperature ranges can be distinguished corresponding to the different degradation steps previously observed in TG analyses. Around 100°C all tested samples release water molecules which are also observed between 200°C and 300°C only for neat (PAH-MMT)₄₀ coatings. The water molecule trapped inside the coatings is released at temperatures higher than 100°C (in correlation with TGA results). In the temperature range from 350°C to 500°C all samples yield methane, ammonia, carbon monoxide, nitric oxide or NH₂CH₂ chains and dioxide carbon or amide or NH₂C₂H₄ chains except the t_{TOF} sample which does not produce ammonia, methane and CO. From 600°C the pristine polyamide 6, neat coatings, coated PA6, t_{25s}, t_{TTI}, t_{pHRR} and t_{TOF} samples release essentially CO₂ or amide or NH₂C₂H₄ chains with additional products such as nitric oxide or NH₂CH₂ chains for coated PA6 and water molecule for both neat coatings and t_{TOF}. From MS results, it could thus be evidenced that during the thermal degradation the polyamide 6 and coatings produce different species including methane, ammonia, carbon monoxide, nitric oxide or NH₂CH₂ chains and dioxide carbon or amide or NH₂C₂H₄. From t_{TOF} no ammonia coming from PAH and polyamide 6 was released which could explain the decrease of interplanar distance between two platelets. In fact during the combustion we degraded both the PAH trapped between clays and the polyamide 6 substrate.

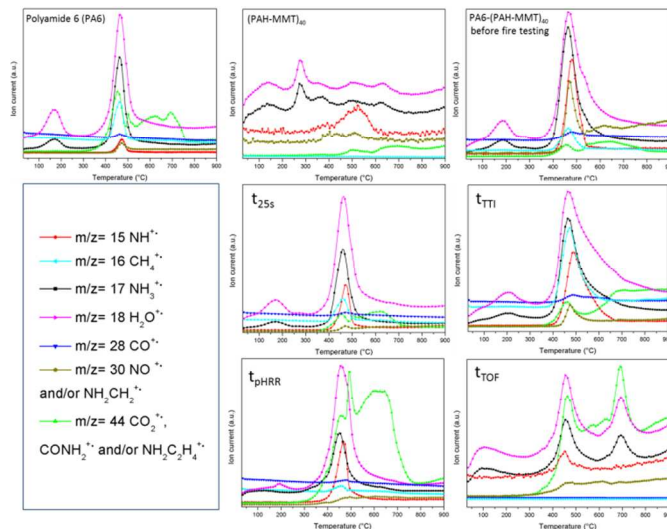


Fig. 13 Mass spectrometric curves of some selected products recorded during the degradation of PA6, (PAH-MMT)₄₀, PA6-(PAH-MMT)₄₀ and specimen residues at 25s, TTI, pHRR and TOF.

In order to check the mode of action of our coatings, PCFC was used to test the fire properties of pristine polyamide 6 and PA6 coated with (PAH-MMT)₄₀ (Fig.14). It is noteworthy that the PCFC technique, measuring the heat release rate (HRR) of the pyrolysis products of the sample, gives us information on the mode of action of flame retardant acting in the gaseous phase. The PCFC data are gathered in Table 4.

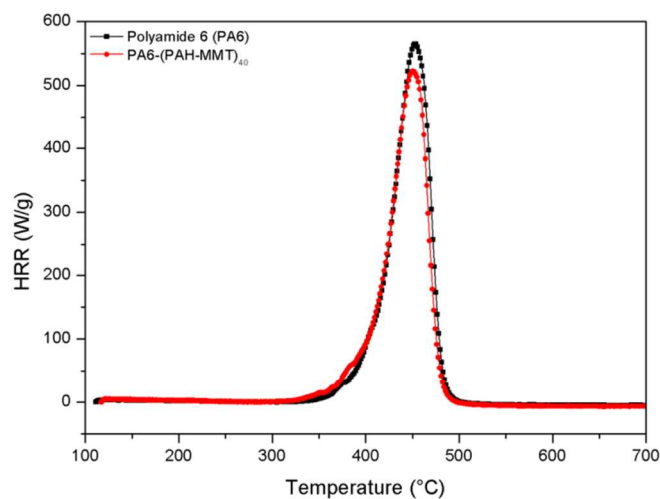


Fig. 14 HRR as function of temperature of pristine polyamide 6 and coated with 40 BL assembly.

	peak HRR (°C)	peak HRR (W/g)	% reduction
Polyamide 6 (PA6)	452 ± 2	568 ± 3	-
PA6-(PAH-MMT) ₄₀	450 ± 2	521 ± 2	8

Table 4 PCFC results for PA6 and PA6-(PAH-MMT)₄₀

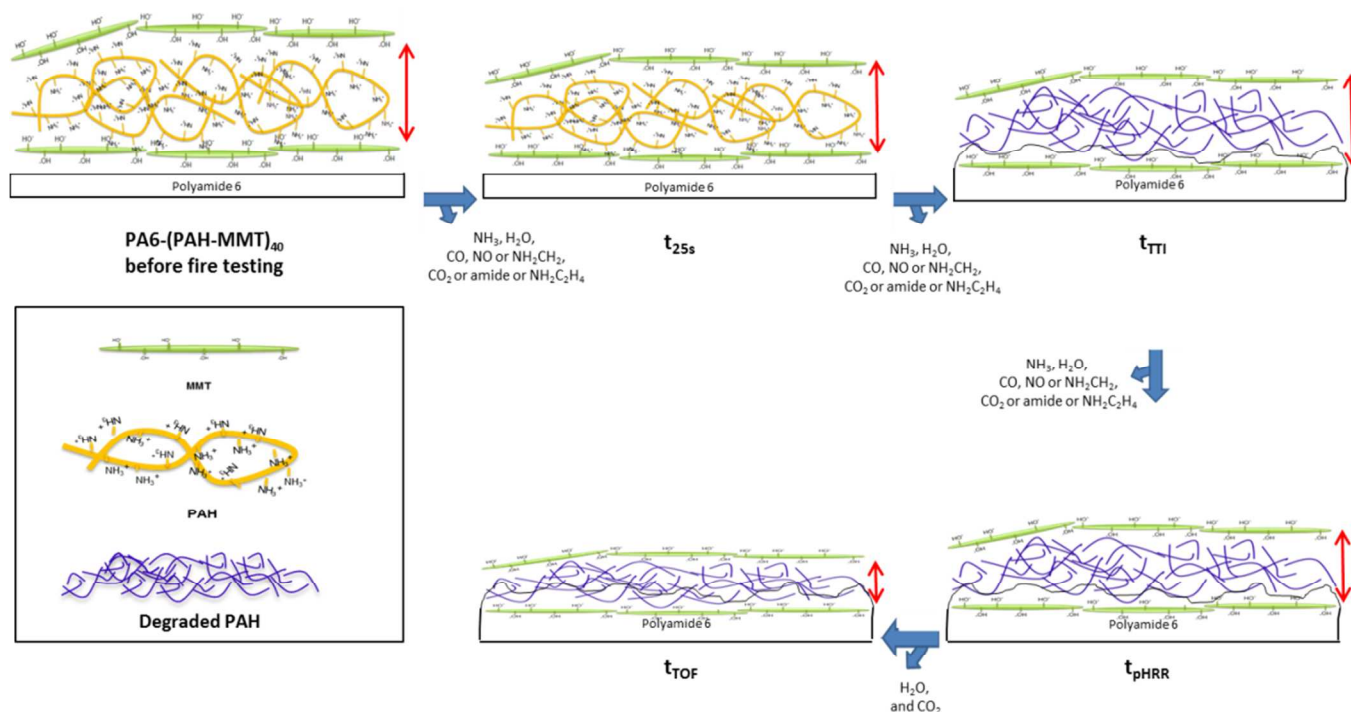
The pristine polyamide fabric displays a maximum pHRR of 568 ± 3 W/g and a decomposition temperature of 452 ± 2°C

on the contrary to coated PA6 which exhibits a maximum pHRR of 521 ± 2 W/g and a decomposition temperature of 450 ± 2 °C. From these findings and previous results obtained in cone calorimeter¹⁰, we have evidenced that the (PAH-MMT)₄₀ coating acts in condensed phase by forming a physical barrier which delays the inflammation of sample.

Conclusions

For the first time, the mechanism of LbL-flame retardant coatings based from poly(allylamine) (PAH) and montmorillonite (MMT), deposited on polyamide 6 (PA6) bulk polymer, has been investigated in this paper (Fig. 15). Throughout this work, different characterization tools have been used to study both condensed and gas phases. Before fire testing, (PAH-MMT) coating presents an ordered lamellar structure as evidenced by SEM observation. XRD results show an increase of the basal spacing of coatings compared to MMT powder. This increase is attributed to the intercalation of polycations (e.g.: PAH¹⁰ or BPEI⁷) between the sheets. Once the cone calorimeter starts, the temperature of the sample increases gradually to reach the temperature of degradation of PAH. At this temperature, the PAH starts to degrade (before polyamide 6) and releases different volatiles products such as ammonia, water, carbon monoxide and dioxide carbon which slows down the ignition of sample.

Furthermore the degradation of PAH was evidenced on the one hand by XRD results with a decrease of basal spacing and on the other hand by LDI results with the detection of new peak series spaced by ± 12 Da. The released products will be maintained in the condensed phase thanks to the appropriate barrier properties of the coating⁹. From TGA results, (PAH-MMT) assembly left (at 900°C) 70 wt% of residue probably due to the MMT⁹ which explains why the thermal diffusivity of the coating is very high compared to pristine substrate. In fact, the higher thermal diffusivity (but also the absorptivity) of the coating would ensure a better dissipation of the heat in the surface and therefore increase the time to ignition. Afterwards the polyamide 6 degrades with also the liberation of volatiles products. Degradation of PAH and polyamide 6 will contribute by their released products to swelling of the carbonaceous char layer formed at the surface of substrate. At the end of combustion (at TOF), according to LDI and ¹³C NMR experiments, we find the presence of degraded PAH but also polyamide 6 which was protected by the coatings. The mode of action of this coating occurs only in the condensed phase as confirmed by PCFC results.



Acknowledgements

Supported by the National Research Fund, Luxembourg (FNR 10/MS/788816).

Notes and references

^a Department for Advanced Materials and Structures, Centre de Recherche Public Henri Tudor, 5 Rue Bommel ZAE Robert Steichen, L-4002, Hautharage. *E.mail: kadir.apaydin@tudor.lu, abdelghani.laachachi@tudor.lu

^b UMET-ISP, UMR 8207, ENSCL, UMET UMR CNRS 8207, CS 90108, 59652 Villeneuve d'Ascq Cedex – France.

† Electronic Supplementary Information (ESI) available: [Mass spectrometry data for montmorillonite, poly(allylamine) and resulting residue at t_{2S} , t_{TTI} , t_{PHRR} and t_{TOF}].

1. F. Carosio, C. Negrell-Guirao, A. Di Blasio, J. Alongi, G. David and G. Camino, *Carbohydrate Polymers*.
2. L. Wang, T. Zhang, H. Yan, M. Peng and Z. Fang, *Journal of Applied Polymer Science*, 2013, **129**, 2986-2997.
3. T. Xu, L. Zhang, Y. Zhong and Z. Mao, *Journal of Applied Polymer Science*, 2014, **131**, n/a-n/a.
4. S. Chang, R. P. Slopek, B. Condon and J. C. Grunlan, *Industrial & Engineering Chemistry Research*, 2014, **53**, 3805-3812.
5. Y.-C. Li, Y.-H. Yang, Y. S. Kim, J. Shields and R. D. Davis, *Green Materials*, 2014.
6. Y. S. Kim and R. Davis, *Thin Solid Films*.
7. Y.-C. Li, J. Schulz, S. Mannen, C. Delhom, B. Condon, S. Chang, M. Zammarano and J. C. Grunlan, *ACS Nano*, 2010, **4**, 3325-3337.
8. G. Laufer, C. Kirkland, A. A. Cain and J. C. Grunlan, *ACS Applied Materials & Interfaces*, 2012, **4**, 1643-1649.
9. A. Laachachi, V. Ball, K. Apaydin, V. Toniazzo and D. Ruch, *Langmuir*, 2011, **27**, 13879-13887.
10. K. Apaydin, A. Laachachi, V. Ball, M. Jimenez, S. Bourbigot, V. Toniazzo and D. Ruch, *Polymer Degradation and Stability*, 2013, **98**, 627-634.
11. M. Strohalm, D. Kavan, P. Novák, M. Volný and V. r. Havlíček, *Analytical Chemistry*, 2010, **82**, 4648-4651.
12. K. Apaydin, A. Laachachi, V. Ball, M. Jimenez, S. Bourbigot, V. Toniazzo and D. Ruch, *Polymer Degradation and Stability*.
13. J. W. Gilman, R. H. Harris, J. R. Shields, T. Kashiwagi and A. B. Morgan, *Polymers for Advanced Technologies*, 2006, **17**, 263-271.
14. P. Verge, T. Fouquet, C. Barrère, V. Toniazzo, D. Ruch and J. A. S. Bomfim, *Composites Science and Technology*, 2013, **79**, 126-132.
15. N. S. Murthy, G. R. Hatfield and J. H. Glans, *Macromolecules*, 1990, **23**, 1342-1346.
16. T. L. Weeding, W. S. Veeman, H. A. Gaur and W. G. B. Huysmans, *Macromolecules*, 1988, **21**, 2028-2032.
17. G. R. Hatfield, J. H. Glans and W. B. Hammond, *Macromolecules*, 1990, **23**, 1654-1658.
18. S. V. Levchik, E. D. Weil and M. Lewin, *Polymer International*, 1999, **48**, 532-557.
19. H. Liu, P. Yuan, Z. Qin, D. Liu, D. Tan, J. Zhu and H. He, *Applied Clay Science*, 2013, **80–81**, 398-406.
20. P. Yuan, P. D. Southon, Z. Liu, M. E. R. Green, J. M. Hook, S. J. Antill and C. J. Kepert, *The Journal of Physical Chemistry C*, 2008, **112**, 15742-15751.
21. H. Seefeldt, E. Duemichen and U. Braun, *Polymer International*, 2013, **62**, 1608-1616.
22. M. Porubská, O. Szöllös, A. Kőňová, I. Janigová, M. Jašková, K. Jomová and I. Chodák, *Polymer Degradation and Stability*, 2012, **97**, 523-531.
23. Y.-C. Li, S. Mannen, A. B. Morgan, S. Chang, Y.-H. Yang, B. Condon and J. C. Grunlan, *Advanced Materials*, 2011, **23**, 3926-3931.
24. C. Isbasar and J. Hacaloglu, *Journal of Analytical and Applied Pyrolysis*, 2012, **98**, 221-230.